DOI:
10.1002/smll.201600465

Document Version
Peer reviewed version

DOI: 10.1002/((please add manuscript number))
Article type: Full Paper

Flexible Asymmetric Encapsulation for Dehydration-Responsive Hybrid Microfibers

*Ankur S. Chaurasia, and Shahriar Sajjadi**

PhD candidate A. S. Chaurasia, Dr. S. Sajjadi
Department of Physics, King's College London, Strand, London, WC2R 2LS, UK
E-mail: shahriar.sajjadi-emami@kcl.ac.uk

Keywords: alginate, microfibers, asymmetric encapsulation, microfluidics, core-release

A new class of smart alginate microfibers with asymmetric oil encapsulates is introduced. These fibers were produced by injecting an aqueous alginate solution into outer aqueous calcium chloride solution to form alginate fibers, which were asymmetrically loaded with oil entities through eccentrically aligned inner capillaries. The fiber morphology and its degree of asymmetry could be tuned via altering the size, location and frequency of the oil encapsulates. These asymmetric fibers revealed significant potential for applications where conventional symmetric fibers failed to perform. We show how asymmetric oil-encapsulated fibers can become dehydrated-sensitive, and trigger the release of encapsulates if their hydration level drops below a critical value. We also show how the triggered-response could be switched-off on demand by stabilizing the oil encapsulates. We demonstrate the capability of asymmetric fibers to carry and release multiple cargos in parallel. The fibers loaded with equal-sized spheres were more asymmetric than those containing unequal drops, had a higher tensile strength and showed a better potential for triggered response.

1. Introduction

Biocompatible calcium-alginate microfibers are widely used in a variety of formats such as non-woven fiber pads and scaffolds, in pharmaceutical and biomedical applications like wound healing[1-3] and tissue engineering.[4,6] The range of applications of alginate microfibers has been extended by tuning the composition and topography of the fibers,[7] and encapsulating various aqueous[8,9] as well as non-aqueous core[10,11] materials in the fibers shell matrix. To further enhance the fiber's multi-functional capabilities, encapsulation of multiple phases has also been reported.[12]

Broadly, the fiber encapsulate morphology can be divided to continuous, as in tubular fibers, and discontinuous or segmented, as in fibers with spherical or plug entities. Geometrically, encapsulation within fibers can be obtained in two ways, symmetric and asymmetric, with respect to the fiber's central axis. The latter configuration can result in fibers with a variety of surface morphologies, particularly in dried state. However, there is almost no information available in the literature regarding asymmetric fibers except for multi-tubular fibers produced via asymmetric injection of multiple aqueous phases in parallel into the gelling alginate phase.[13,14] While symmetric fibers enjoy from uniformity in structure and morphology, which is ideal for many applications, they suffer from lack of versatility in dealing with novel applications where encapsulate interaction or rupture is sought, or fibers with variant morphology are desired.

The conventional *two-step* encapsulation strategy,[15,16] where the oil droplets are formed prior to their encapsulation, can only produce fully concentric or symmetric encapsulation of the oil droplets, even if the droplets are produced asymmetrically, as shown in **Figure 1**a1. This is because the oil droplets initially formed upstream in asymmetric positions, tend to move to the central axial location, before being encapsulated at a considerable distance downstream. This has been observed even in the case of simultaneous asymmetric injection of two parallel oil

streams,[10] a schematic of which is shown in Figure 1a2. The resulting symmetric fibers, examples of which are shown in Figure 1b, trap the oil encapsulates upon dehydration (Figure 1c-1d) and retain their symmetry.

We introduce a facile microfluidic approach for tunable asymmetric encapsulation of oil in alginate microfibers, based on the simultaneous (*one-step*) formation and encapsulation approach, where the droplets are directly trapped within the gelling fiber in desired locations. A number of potential applications are suggested for asymmetric fibers. We show that the oil cores can be trigger released upon dehydration of the microfiber having asymmetric encapsulates. We further demonstrate the capability of such fibers to carry and release multiple cargos in parallel.

2. Results and Discussion

2.1 Fabrication of asymmetric fibers

To produce asymmetric fibers, we merged the two distinct steps, drop formation and encapsulation, usually used for the fabrication of encapsulated fibers, into a *one-step* process (**Figure 2**a1) where the droplets were formed directly into the gelling fiber. This approach instantly locked the droplets inside the gelled fiber at the locations they were formed, thus preventing their movements. This single-step strategy also allowed for the droplets to be loaded asymmetrically, as shown in Figure 2a1. A typical resulting asymmetric fiber is shown in Figure 2c1.

The composition and functionality of the asymmetric fibers can be further enhanced by encapsulating more than one type of hydrophobic materials in a single fiber. The realization of such a hybrid fiber architecture has previously been demonstrated by Yu et al.[10] with the use of an intricate *two-step* approach coupled with digitally controlled valves and additional

compensatory flows of the alginate phase. However, this approach also produced symmetric fibers with linearly arranged compound droplet sequences. To fabricate asymmetric fibers with two kinds of hydrophobic encapsulates, we extended our *one-step* encapsulation strategy by using two parallel inner glass capillaries to form two independent sequences of droplets, directly fed into a gelling alginate fiber (Figure 2a2). The tip cross-section of the device is shown in Figure 2d, while a typical hybrid asymmetric fiber encapsulating two droplet sequences is shown in Figure 2c2.

The droplet size, frequency and location in each stream can be individually manipulated to tune the surface morphology of asymmetric fibers. The droplet size of each stream can be independently adjusted with the corresponding oil phase flow rate, without affecting the size of its neighboring droplet sequence. However, this may affect the asymmetry of the encapsulated droplets with respect to the fiber's axis. This is illustrated in **Figure 3**a, where only the flow rate of the left stream (light-colored) increased to: 0.125, 0.25, 0.50, 1.0, 2.0, 4.0 and 6.0 mlh^{-1}, while the flow rate of the right stream (dark-colored) was fixed at 1.0 mlh^{-1}.

We quantify the degree of asymmetry of the fibers by defining a characteristic angle, the angle of asymmetry (θ), which is the angle between the line of fiber's axial symmetry and the line connecting the centers of two adjacent droplets, as shown in Figure 3b. A higher θ reflects a more asymmetric positioning of droplets within the fiber. The degree of asymmetry rapidly decreased with increasing oil phase ratio ([% $\phi_{oil} = 100 \times Q_{oil} / (Q_{oil} + Q_{alg})$]), as shown in Figure 3c. The angle of asymmetry for equal-sized adjacent oil spheres (θ_e) was higher than the angle for unequal spheres (θ_u) at low $\boldsymbol{\phi_{oil}}$, as shown in Figure 3c, but they were the same ($\theta_e = \theta_u$) at high ϕ_{oil}. The maximum angle of asymmetry achieved was ~30º for equal oil spheres with diameters around 2/3 of the fiber diameter (Figure 3a3-3a4). The asymmetric surface morphology of these fibers can be clearly seen from the SEM images shown in Figure 3a4 (inset). The arrangement of droplets with unequal size from parallel streams became less

asymmetric due to increased interaction between the two oil phases, until eventually the formation of asymmetric encapsulates became impossible as the droplets tended to arrange linearly and symmetrically (Figure 3a6).

This loss of fiber asymmetry could be revived by minimizing the interaction between the two oil streams, for example by inclusion of the tubular and segmented oil encapsulates in the fibers. This was achieved by reducing the size of spherical droplets in one stream, via increasing the alginate phase flow rate, which minimized their interactions with the adjacent oil stream and allowed it to evolve as a tubular jet (Figure 3d2). The phase interaction was fully suppressed at a higher alginate phase flow rate resulting in the formation of fibers containing a smooth tubular oil phase in parallel with oil droplets (Figure 3d3). These fibers, as shown in Figure 3f1, benefit from having both encapsulation geometries, where tubular geometry provides a high encapsulation volume, while segmented geometry provides robustness against complete oil loss in the event of fiber split. The fiber takes an asymmetric surface profile upon dehydration, with a smooth surface around the tubular oil section and a wavy profile around the segmented oil droplets (Figure 3f2). Such a fiber, when split, releases the oil from only the tubular section, while the segmented oil droplets remain trapped in the fiber, as shown in Figure 3f3-3f5.

Increasing the volumetric flow rates of both oil streams to a great extent intensified the interaction between them, which further compromised the fiber's asymmetry, and led to the formation of fibers with highly packed linearly-arranged alternating oil plugs (**Figure 4**a). Due to the closely packed oil plugs, the fiber's surface appeared to be flat upon dehydration (Figure 4b3 and 4c3), a feature not observed for the symmetric fibers made by conventional methods, examples of which are shown in Figure 1d. However, fibers with densely-packed oil plugs enjoy a high oil phase ratio (ϕ_{oil}), which can be only paralleled with fibers with tubular oil geometry (Figure 3f). Tubular fibers suffer from a risk of core loss in case of a single accidental shell rupture, while the fibers with plug encapsulates are highly robust against this drawback.

However, this advantage comes at the cost of a reduction in tensile strength. We compared the tensile strength of a densely-packed plug fiber (ϕ_{oil} = 84%) against a tubular fiber with the same oil phase ratio, and found that the tubular fiber resisted a higher tensile force than a highly-packed plug fiber (Figure 4d). This is because a tubular geometry enjoys a large and uniform shell thickness, as all the alginate hydrogel contributes to the fiber's shell formation, unlike the plug fiber which contains alginate films separating adjacent oil plugs.

2.2 Asymmetric fibers for advanced fiber assembly

Figure 5 shows three classes of custom-designed asymmetric fibers produced using the proposed one-step asymmetric encapsulation technique. Figure 6a and 6b represent asymmetric fibers with linear and alternating encapsulates, respectively, while Figure 6c shows Janus-like fibers. Fibers with customized morphologies can be used as building blocks for fabricating hybrid fiber films or pads for usage in biomedical applications such as wound healing.[1-3] For such applications, the accurate handling and precise arrangement of individual fibers, to prevent unwanted fiber twisting and fractures, are some of the major practical challenges to be resolved. However, recent developments in fiber manipulation techniques, such as magnetic manipulation of fibers via encapsulation of magnetic mineral oil solution,[16] could provide a controlled methodology for desired fiber manipulation of individual fibers.

The simplest type of asymmetric fiber, which consists of a single sequence of asymmetric oil-encapsulates, has a flat surface on one side and a wavy morphology on the other (Figure 5a1). Two such fibers could be intertwined in two geometrically different ways, the alternating asymmetric arrangement and the interlocking 'clicked-fiber' arrangement (Figure 5a2), to produce thin alginate sheets. These two configurations can be further arranged to prepare four different fiber pads.

A more complex fiber structure consisting of two sequences of asymmetric encapsulates can be directly produced by synchronizing the droplets frequency. To make fibers with alternating

asymmetric morphology, large droplets at a low frequency were produced (Figure 5b1). A pair of these fibers can be combined to produce a fibrous building block having symmetric wavy morphology with configurable oil compositions, as shown in Figure 5b2. These fibers can be intertwined to create two varieties of fiber pads. If oil droplets from the two streams can be generated simultaneously while their size being controlled to be smaller than the half of the alginate fiber, then it would be possible to produce Janus-like structures as shown in Figure 5c1, which can be arranged to produce two additional varieties of fiber pads. Asymmetric fibers with two sequences have higher tensile strength than those with single stream at a given oil phase ratio ϕ_{oil} (Figure 5d). Fibers with two oil streams contained droplets which were smaller than the single droplets formed in the fibers with one stream. A large droplet size in a single stream resulted in an extremely thin ‘minimum‘ shell thickness, as schematically indicated by the red arrows in Figure 5d, which made the fiber weaker. Overall, the proposed *one-step* oil-encapsulation strategy is capable of fabricating asymmetric as well as symmetric hybrid alginate microfibers with a wide variety of morphologies.

2.3 Dehydration-responsive asymmetric microfibers

All encapsulated alginate fibers, asymmetric and symmetric, can undergo controlled-release in wet state where the drug can diffuse out through the alginate porous shell with a rate depending on the pore size, solubility, and other conditions. In this research we seek for a complementary mechanism that allows a burst release in dry state. There is no report in the literature that demonstrates a burst-release mechanism from oil-loaded alginate fibers in dried state. The only burst-release mechanism reported in the literature is via dissolution (or uncrosslinking) of the fiber’s shell in the wet state and in the presence of sodium citrate.[12]

Before moving on to demonstrate the release mechanism, we first show how the conventionally oil-loaded alginate fibers respond upon dehydration. The dehydrated symmetric fibers, shown

in Figure 1c-1d, were stable and maintained their encapsulated entities with time irrespective to the segment shape, which is consistent with previous observation.[10]

Asymmetric fibers are potentially prone to shell rupture by dehydration due to asymmetric stresses applied on the fiber shell during contraction, which tend to break the shell and release the cores if sufficient stress is generated. We first studied fibers with a single and two stream of asymmetrically encapsulated oil segments, as shown in Figure 5a-5c. None of the fibers shell did rupture upon dehydration. However, when the oil droplets from two streams were alternatively produced and closely packed in the fiber (**Figure 6**a1), the dehydration-responsive feature emerged. Every pair of oil droplets in these fibers underwent arrested coalescence. This resulted in a series of inclined dumbbell-shaped oil segments (Figure 6a2) that ruptured the shell upon drying, as shown in Figure 6a7. We found that the angle of asymmetry θ determines whether the core would be released upon fiber dehydration. For example, the fibers with $\theta <$ ~15º (Figure 3a5-3a6) failed to release the core upon drying, as the volume of one droplet became too large in comparison to the other, which made the fiber lose its asymmetry. In addition to requirement of having an optimum inter-droplet size-proportion of ~ 1.5:1.0 for retaining the fiber asymmetry, the droplet size in both streams should be less than ~2/3 of the fiber diameter, but not less than 1/2 of fiber diameter, otherwise droplets may come directly on top of each other, as shown in Figure 5c1. The dehydration-responsive fibers were quite resilient in hydrated state and contained the oil droplets for a minimum of seven months without undergoing any undesirable release via leakage. The fibers were also found to be robust against storage in pure water for several months, as they did not lose their responsive function.

The release behavior was analyzed by monitoring the time-evolution of the weight of a sample responsive fiber during its dehydration. This weight-evolution was compared against a similar curve for a non-responsive fiber (Figure 6e), where the oil droplets were stabilized by the addition of surfactant (1.0 wt% Tween20) to the alginate phase. Both samples were prepared

using identical flow conditions and formulation. Figure 6d shows the reduction in the fiber weight during the dehydration process for both responsive and non-responsive fibers. The weight of the responsive fiber settled down to a smaller value than that for the non-responsive fiber, as the oil released from the fiber evaporated. The instance of the shell rupture and the concomitant oil-release can be understood as the point of deflection between the two curves (Figure 6d inset). The difference between the weights of the two fibers after 2h of drying at room temperature (~3.20 mg) was found to be nearly equal to the weight of the oil encapsulated in the sample fiber (~3.26 mg). The inset graph reveals that the onset of shell rupture and also the time taken for the released oil to completely evaporate correlates well with the time-scale shown in Figure 6a. For this particular fiber, the swelling ratio at the instance of the shell rupture (S_{rup}) was found to be ~15% of the saturation swelling ratio (S_{sat}). This implies the fibers released oil when their water content fell below 15% of their maximum water intake.

The release feature of any single dumbbell was independent of other dumbbells across the fiber. This means that the oil content (encapsulated volume) of these responsive fibers could be easily tailored by generating the droplets at a reduced frequency, as shown in Figure 6c1, while the responsive feature is preserved, as shown in Figure 6c3.

The responsive microfibers could only be formed within a narrow range of alginate concentration (1 ± ~0.25 wt%) under the conditions of this study. We explored that a too low alginate concentration would allow a rapid coalescence of the adjacent oil droplets, thus preventing the formation of the inclined dumbbell-shaped oil segments, which was a pre-requisite to rupture the shell upon dehydration. On the other hand, a high alginate concentration was found to result in a strong alginate shell around the oil droplets, which resisted the shell rupture upon dehydration (Figure 6e). Additionally, the spacing between the two inner tips, and their location relative to the outer capillary tip also played important roles in the formation of fibers. If the two inner capillaries were too close (< ~20μm), the parallel oil phases coalesced

prior to droplet formation. On the other hand, if the two tips were far apart from each other, implying that they were too close to the outer capillary tip (< ~40µm), the droplets escaped out of the alginate phase before gelation could occur. In spite of this narrow range of formulation and flow conditions, there exists an operational window within which the onset of rupture, in terms of fiber hydration level, can be adjusted. Such tailored responsive fibers with a graded release threshold could open up opportunities for moisture monitoring in wound healing applications.

We demonstrated a convenient and benign dehydration-triggered core-release mechanism using a model hydrocarbon oil (Octane) as core material. However, this can be extended to appropriate biocompatible oils or oil-based anti-microbial and anti-inflammatory ointments like essential oils [2] and hormones.[17,18] The proposed dehydration-triggered core-release mechanism is particularly designed for smart burst-release applications in dried state and in the absence of dispersion media. A non-woven pad made of asymmetric fibers will find usage for dry wounds or in the later stage of wound healing process when the wound begins to dry, and anti-microbial ointments need to be applied, therefore providing a rapid, hands-free treatment. Asymmetric alginate fibers can also be used for controlled-drug release in wet state too, as they have the same chemical structure as symmetric fibers, but they have the potential to undergo burst release when the wound/fiber dries up in the later stage of healing.

One can imagine that for applications which demand simultaneous release of two or more components, a bundle of mixed responsive fibers can be used, where the release of two components occur from different fibers. However, a smart design would involve the concomitant release of the two components from a single fiber. Here, we demonstrate that the proposed release mechanism can be extended further to include the triggered release of two components, which confers multi-functionality to such responsive fibers. We demonstrate this by loading two sequences of different oil droplets, similar to that shown in Figure 6a1. We can see from Figure 6b1 that all (non-coalescing) pairs of droplets take an inclined dumbbell-like

morphology when they come to close contact, which is the requirement for dehydration-induced release. To maintain the droplets identity, the droplet coalescence should be avoided prior to release. This poses a formidable task, because while the presence of surfactant can hinder coalescence, results show that it may also make the fibers non-responsive to dehydration because of improved stability of the inclusions. A wide range of surfactant concentrations in the middle alginate phase was investigated, and it was found that using an extremely small concentration of surfactant (0.01 wt% Tween 20) in the alginate phase was sufficient to prevent the coalescence (Figure 6b1), yet low enough to allow the shell to rupture upon dehydration (Figure 6b4-b8).

An interesting feature emerges when the responsive mode of these asymmetric fibers is switched off by stabilizing the droplets with surfactants. The resulting fibers release the content from two adjacent compartments at the point of rupture when split via a rapid tensile pulling (Figure 6e4). This occured due to the asymmetrically encapsulated droplets which, when dehydrated, gradually evolved into an array of close-packed compartments in a zigzag fashion (Figure 6e3). It is worth noting that oil-encapsulated microfibers having a linear arrangement for the adjacent compartments[10-12,15,16], fail to rupture adjacent compartments when they are split. This feature of asymmetric fibres can be taken advantage of when a two-component release is desired.

The dehydration-responsive fibers can also be potentially used for constructing complex fibrous structures, such as 3D fiber scaffolds[19-22], in addition to wound healing pads. For such applications, fibers should also possess sufficient tensile strength to avoid accidental mechanical fractures and breakages during their handling and operation. We conducted uniaxial tensile testing of dehydrated asymmetric fibers for identifying the optimum encapsulate geometry and arrangements to maximize the fiber strength. These tests were performed using

non-responsive fibers, but with exactly the same morphology and composition, to avoid the impact of the shell fracture due to the fiber dehydration during tensile testing.

Fibers with the lowest oil-volume fraction (ϕ_{oil}) withstood the highest tensile force, as shown in Figure 6f. This is reasonable because the alginate shell thickness, which contributes to the fibers strength, increased with decreasing ϕ_{oil}. Interestingly, a more asymmetric fiber could be produced by decreasing ϕ_{oil}, as indicated by the associated increase in θ (Figure 3c).

To further refine the ideal requirement for designing dehydration-responsive fibers, we compared tensile strength of asymmetric fibers with equal and unequal sized spheres at a fixed low ϕ_{oil} of 40%, as shown in Figure 6g. The fiber with equal-sized spheres resisted a higher tensile force, owing to a larger ‘minimum‘ shell thickness resulting from the small-sized droplets, as schematically indicated by the red arrows in Figure 6g. Fibers with equal-sized spheres were also more asymmetric (larger θ) than their counterparts with unequal droplet sizes, as observed previously in Figure 3c.

From these two analyses, we conclude that asymmetric dehydration-responsive fibers loaded with a lower volume of oil and having equal-sized spheres are more asymmetric and have a higher tensile strength, provided that the adjacent droplets remain in touch with each other.

Conclusion

A flexible one-step microfluidic approach was introduced for the fabrication of hybrid oil-encapsulated alginate microfibers with asymmetric encapsulates. Fibers with custom-designed internal architectures were produced by direct wet spinning and configuring the encapsulate location, size and frequency. In addition, strategies for intertwining these fibrous building blocks to create complex fiber assemblies were also demonstrated.

An application of symmetric fibers was exhibited by fabricating dehydration-responsive microfibers which displayed a core-release mechanism triggered by dehydration of the hydrogel shell. The compound shape of oil segments, achieved due to asymmetric encapsulation, promoted the shell rupture upon dehydration, but could be muted by adding surfactants to the alginate phase if required. The dehydration-induced release mechanism was also extended to fibers with double oil cargos. Several factors, such as the formulation and device configuration, affected the fabrication of dehydration-responsive microfibers. Fibers with equal-sized oil spheres displayed a higher angle of asymmetry than those loaded with unequal spheres at a low ϕ_{oil}, and also had a higher tensile strength.

Experimental Section

Materials: The middle phase constituted an aqueous solution of 1 wt% sodium alginate, while the outer aqueous bath contained 4 wt% calcium chloride. Octane (99%, Sigma Aldrich) was used as received as the model inner-oil encapsulated phase. Sodium alginate and calcium chloride (Sigma Aldrich) were used as received. Sudan Red and Sudan Black (FastColours UK) were used as the oil-soluble dyes. Sodium dodecyl sulfate (SDS) and Tween 20 were used as water-soluble surfactants (Sigma Aldrich).

Device: Figure 2a shows two schematics of the different microfluidic device configurations used to encapsulate oil within the alginate fiber. The device fabricated as per the configuration shown in Figure 2a1 used two glass capillaries, circular (ID: 0.56 mm, OD: 1 mm) and square (IL: 1 mm, OL: 1.5 mm). The inner capillary was pulled using a pipette puller (P-1000, Sutter Instrument, Novato, USA). The tapered tips were cut to the desired sizes, after which the inner capillary tip (ID: 40 µm, OD: 60 µm) was aligned non-axisymmetrically towards the left edge of the outer capillary tip, with the outer tip (ID: 150 µm, OD: 175 µm). Both capillaries were plasma treated (Femto Plasma Cleaner, Diener) to be hydrophilic. The oil phase was pumped

(Harvard Apparatus pumps) through the inner capillary, while the alginate phase was introduced through the interstitial spaces between the two capillaries. The coupled capillary setup was introduced vertically in a cuvette, which housed the quiescent outer aqueous phase containing calcium chloride as shown in Figure 2a1.

The device fabrication for the second configuration (Figure 2a2) was done using a completely different approach, since the tips of two tapered capillaries could not be inserted together inside the outer tapered capillary. The straight forward use of parallel straight capillaries was also not feasible, as the thin and long capillary (with OD: 80μm) was very flexible, and its tip could not be fixed at a particular location. To circumvent this problem, multiple straight capillaries were assembled to make compound inner capillaries for two inner oil phases, as shown in Figure 2b1. Two such assembled capillaries were inserted in a tapered supporting capillary (Figure 2b2), with the two tips protruding ~2 mm outside the tapered tip of the supporting capillary. The two tips were aligned at a same level and at a fixed distance from each other (~40 μm), and immobilized by the glue applied on both ends of the supporting capillary. This compound assembly was introduced inside a tapered outer capillary, and the coupled inner tips were aligned at the same level as that of the outer capillary, as shown in Figure 2d.

The resulting fibers were collected at the top of the cuvette, facilitated by the buoyancy force exerted by the encapsulated oil. This buoyancy-assisted non-confined microfluidic device has previously been used to generate millimetric core-shell drops.[23,24] A high-speed video recording camera (Photron FastCam SA-5 (monochrome)) was used to record the fiber formation.

The drying behavior of the fiber was monitored by measuring the variation in the weight of a given fiber at room temperature. Precautions were taken to ensure the excess volume of water adhering on fiber external surface was removed, by placing the sample on a piece of water absorbing paper, prior to weighing. The saturation swelling ratio of fibers (S_{sat}), expressed

as $S_{sat} = \left(\frac{w_{wet}-w_{dry}}{w_{dry}}\right)$, was calculated by measuring the weight of a fully hydrated (w_{wet}) and fully dried (w_{dry}) simple alginate fiber. Fiber drying occurred in an oven to a constant weight at 70℃. The saturation swelling ratio for the alginate fiber was found to be ~10.1. The swelling ratio at which the shell rupture occurs is given by $s_{rup} = \frac{w_r \times 100}{S_{swell}}$, where w_r is the weight of water remaining in the gel at the instance of shell rupture, which was calculated via $w_r = w_{wet} - w_{oil} - w_{dry}$. Typical values of w_{wet}, w_{dry}, and w_{oil} for a given length of the fiber chosen for presentation in Figure 6d were 8.10, 3.2, and ~0.3 mg, respectively.

The uniaxial tensile testing of the individual non-responsive asymmetric fibers was conducted using a highly sensitive force-sensing device (DCA-100, First Ten Angstroms), which was operated through its computer software. The device has an immobile metal hanger on its top surface, which is coupled with a built-in force sensing system. The bottom stage can be moved vertically at a specified velocity via an integrated stepper motor. All fibers were cut to a fixed length of 3 cm, and mounted with their two ends strongly secured onto the top and bottom stage. The uniaxial tensile testing was performed by moving the bottom stage down at a fixed velocity (0.2 mm/s) until the fibers split. The tensile testing of individual fibers has also been reported previously for synthetic,[25] as well as simple and composite hydrogel fibers.[15,26-28]

Acknowledgements

We acknowledge the use made of Photron FastCam SA-5 (monochrome) high-speed video recording system, which was borrowed from the EPSRC (Engineering and Physical Sciences and Research Council) Engineering Instrument Pool. We thank Dr. Dimitris Josephides for critical inputs in the device fabrication process during the conception of the project.

Received: ((will be filled in by the editorial staff))

Revised: ((will be filled in by the editorial staff))

Published online: ((will be filled in by the editorial staff))

[1] R. Mahsood, M. Miraftab, *J. Wound Care*, **2014**, 23,153.

[2] I. Liakos, L. Rizzello, D.J. Scurr, P.P. Pompa, I.S. Bayer, A. Athanassiou, *Int. J. Pharm.*, **2014**, 463, 2, 137.

[3] S. Y. Ahn, C. H. Mun, S. H. Lee, *RSC Adv.*, **2015**, 5, 20, 15172.

[4] K.H. Lee, S.J. Shin, Y. Park, S. Lee, *Small*, **2009**, 5, 11, 1264.

[5] H. Onoe, S. Takeuchi, *Drug Discov. Today*, **2015**, 20, 2, 236.

[6] M. A. Daniele, D. A. Boyd, A. A. Adams, F. S. Ligler, *Adv. Healthcare Mater.*, **2015**, 4, 1.

[7] E. Kang, G.S. Jeong, Y.Y. Choi, K.H. Lee, A. Khademhosseini, S.H. Lee, *Nature Mater.*, **2011**, 10, 877.

[8] H. Onoe, T. Okitsu, A. Itou, M. Kato-Negishi, R. Gojo, D. Kiriya, K. Sato, S. Miura, S. Iwanaga, K. Kuribayashi-Shigetomi, Y.T. Matsunaga, Y. Shimoyama, S. Takeuchi, *Nature Mater.*, **2013**, 12, 6, 584.

[9] B.G. Chung, K. Lee, A. Khademhosseini, S. Lee, *Lab Chip*, **2012**, 12, 1, 45.

[10] Y. Yu, H. Wen, J. Ma, S. Lykkemark, H. Xu, J. Qin, *Adv. Mater.*, **2014**, 26, 16, 2494.

[11] X. He, W. Wang, Y. Liu, M. Jiang, F. Wu, K. Deng, Z. Liu, X. Ju, R. Xie, L. Chu, *ACS Appl. Mater. Inter.*, **2015**, 7, 31, 17471.

[12] E. Um, J. K. Nunes, T. Pico, H. A. Stone, *J. Mater. Chem. B*, **2014**, 2, 45, 7866.

[13] Y. Cheng, F. Zheng, J. Lu, L. Shang, Z. Xie, Y. Zhao, Y. Chen, Z. Gu, *Adv. Mater.*, **2014**, 26, 30, 5184.

[14] Y. Cheng, Y. Yu, F. Fu, J. Wang, L. Shang, Z. Gu, Y. Zhao, *ACS Appl. Mater. Inter.*, **2016**, 8, 2, 1080.

[15] X. He, W. Wang, K. Deng, R. Xie, X. Ju, Z. Liu, L. Chu, *RSC Adv.*, **2015**, 5, 2, 928.

[16] T. Sun, C. Hu, M. Nakajima, M. Takeuchi, M. Seki, T. Yue, Q. Shi, T. Fukuda, Q. Huang, *Microfluid. Nanofluid.*, **2015**, 18, 5-6, 1177.

[17] K. Ganguly, K. Chaturvedi, U. A. More, M. A. Nadagouda, T. M. Aminabhavi, *J. Control. Release*, **2014**, 193, 162.

[18] M. G. Chinwala, S. Lin, *Pharm. Dev. Technol.*, **2015**, 16, 2, 403.

[19] Y. Luo, A. Lode and M. Gelinsky, *Adv. Healthcare Mater.*, **2013**, 2, 6, 777-783.

[20] J.F. Mano, G.A. Silva, H.S. Azevedo, P.B. Malafaya, R.A. Sousa, S.S. Silva, L.F. Boesel, J.M. Oliveira, T.C. Santos, A.P. Marques, N.M. Neves and R.L. Reis, *J. R. Soc. Interface*, **2007**, 4, 17, 999-1030.

[21] Z. Izadifar, X. Chen and W. Kulyk, *J. Funct. Biomater.*, **2012**, 3, 4, 799-838.

[22] C. Colosi, M. Costantini, R. Latini, S. Ciccarelli, A. Stampella, A. Barbetta, M. Massimi, L.C. Devirgiliis and M. Dentini, *J. Mater. Chem. B*, **2014**, 2, 39, 6779-6791.

[23] A. S. Chaurasia, S. Sajjadi, *Chem. Eng. Sci.*, **2015**, 129, 260.

[24] A. S. Chaurasia, D. N. Josephides, S. Sajjadi, *ChemPhysChem*, **2015**, 16, 2, 403.

[25] K.A. Kwon, R. J. Shipley, M. Edirisinghe, D. G. Ezra, G. E. Rose, A. W. Rayment, S. M. Best and R. E. Cameron, *Mater. Sci. Eng. C*, **2014**, 35, 220–230.

[26] A. Mirabedini, J. Foroughi, T. Romeo and G.G. Wallace, *Macromol. Mater. Eng.*, **2015**, 300, 12, 1217-1225.

[27] K. Dey, R.A. Khan, A.M.S. Chowdhury, *Polym. Plast. Technol. Eng.*, **2011**, 50, 7, 698-704.

[28] L. Liu, L. Jiang, G.K. Xu, C. Ma, X.G. Yang and J.M. Yao, *J. Mater. Chem. B*, **2014**, 2, 43, 7596-7604.

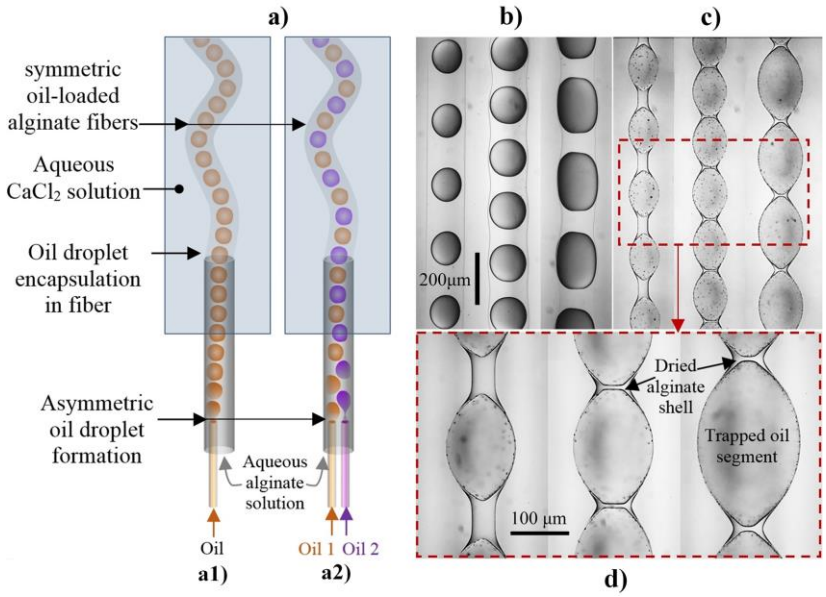

Figure 1 a) Schematics of two conventional microfluidic device-configurations used to produce symmetric oil-encapsulated alginate fibers with different one or more types of linearly arranged oil droplets. The micrographs of hydrated **(b)** and dehydrated **(c)** symmetric fibers are shown, while **(d)** shows a zoomed-in micrograph of the fibers. Scale bar shown in (b) is also applicable for (c).

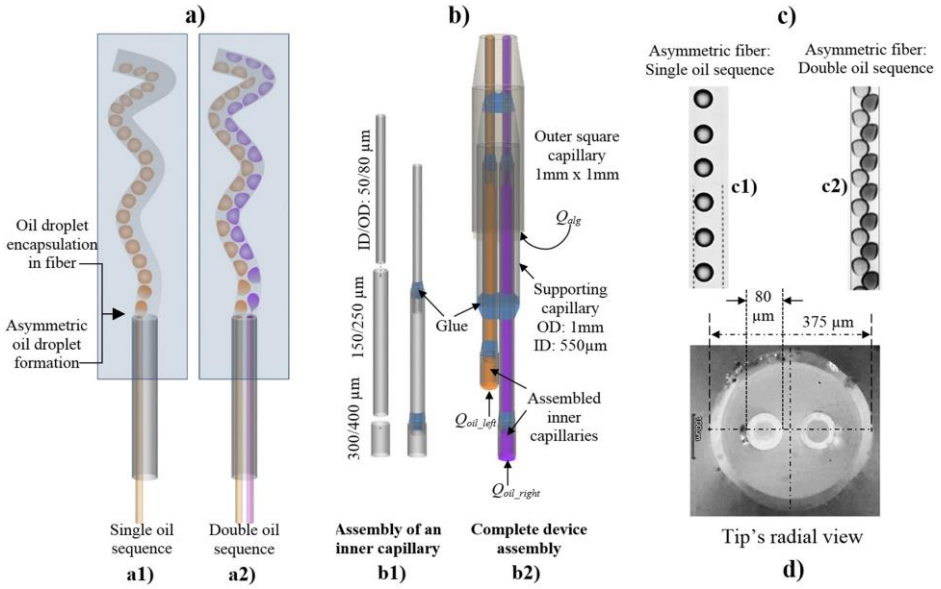

Figure 2 a) Schematics of two microfluidic device configurations, based on simultaneous droplet formation and encapsulation, used to produce oil-encapsulated alginate fibers with one-component non-asymmetric (a1), and two-component non-asymmetric (a2) oil encapsulates. **b)** The schematic shows a glass micro-capillary assembly (b1), and the overall assembly of the microfluidic device (b2) for asymmetric oil encapsulation. **c)** Optical micrographs of a typical one-component asymmetric (c1) and two-component asymmetric (c2) fiber are shown, which were produced using the configurations shown in a1 and a2, respectively. **d)** The tip cross-section of the assembled device.

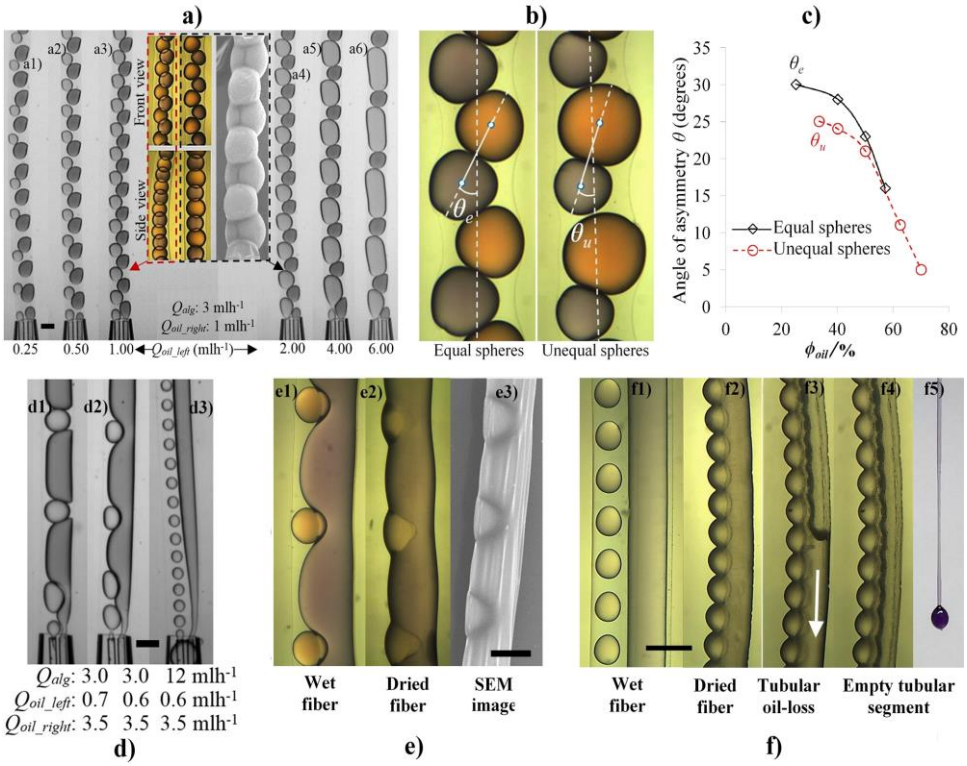

Figure 3 a) The formation of alginate fibers with two-component asymmetric oil encapsulation and the evolution of encapsulate asymmetry with the oil phase flow rate are shown. The left-sided oil droplets are dyed with Sudan Red (FastColours UK), while the right ones are dyed with Sudan Black (FastColours UK). The two sets of inset images in the center (a7) show the front view (top) and the side view (bottom) of two such fibers (shown in a3 and a4) in the hydrated state. The SEM image of a dried asymmetric fiber (a4) is also shown in a7. **b)** The angle of asymmetry (θ) is defined for fibers with equal (θ_e) and unequal (θ_u) spheres. **c)** The graph shows the variation in θ_e and θ_u with oil phase ratio (ϕ_{oil}). **d)** The micrographs show that a symmetric fiber can be turned into asymmetric fiber by altering droplet size on the left stream (d2), whose wet and dry state images are also shown in **(e)**. A more defined encapsulation of tubular and spherical droplets can be easily achieved by decreasing the droplet size and tubular width via increasing Q_{alg} (d3). **f)** The fiber having tubular and spherical encapsulates in wet and dry states are shown in (f1) and (f2) respectively. If such a fiber is split, the oil from tubular encapsulate escapes while the segmented encapsulates remain trapped (f3-f5). All scale bars are 200µm.

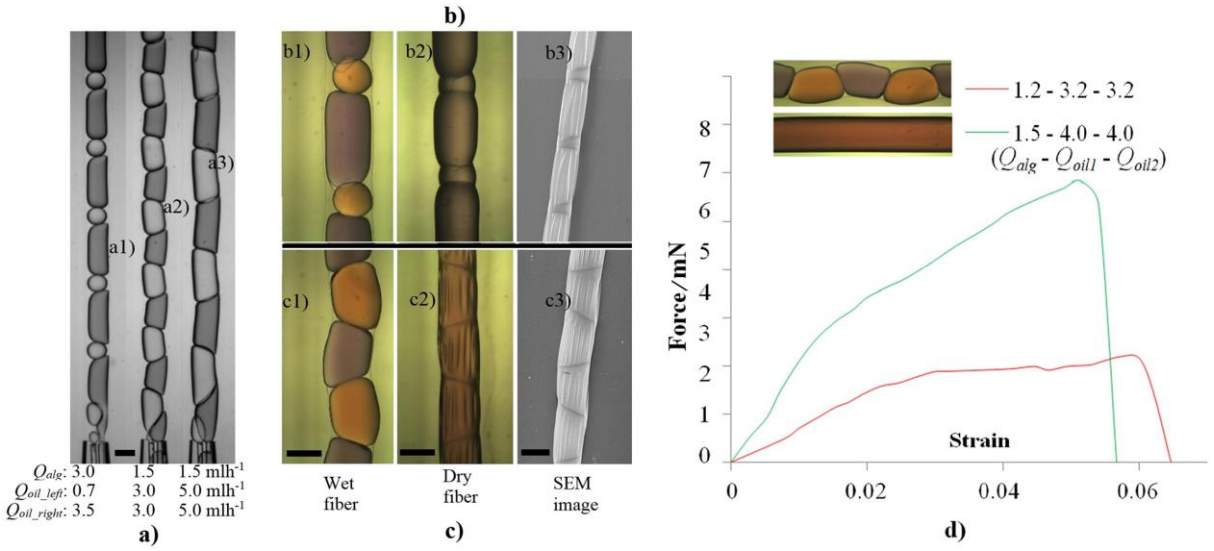

Figure 4 a) Compound oil-loaded algiante fibers with symmetric morphology obtained at increased size of both encapsulates are presented. The morphology of fibers shown in (a1) and (a2) under hydrated and dehydrated states are also shown in **(b)** and **(c)** respectively. All scale bars are 200µm. **d)** A comparison of the force-strain relationship between a highly-packed plug fiber and a tubular fiber with identical oil phase ratio (84%).

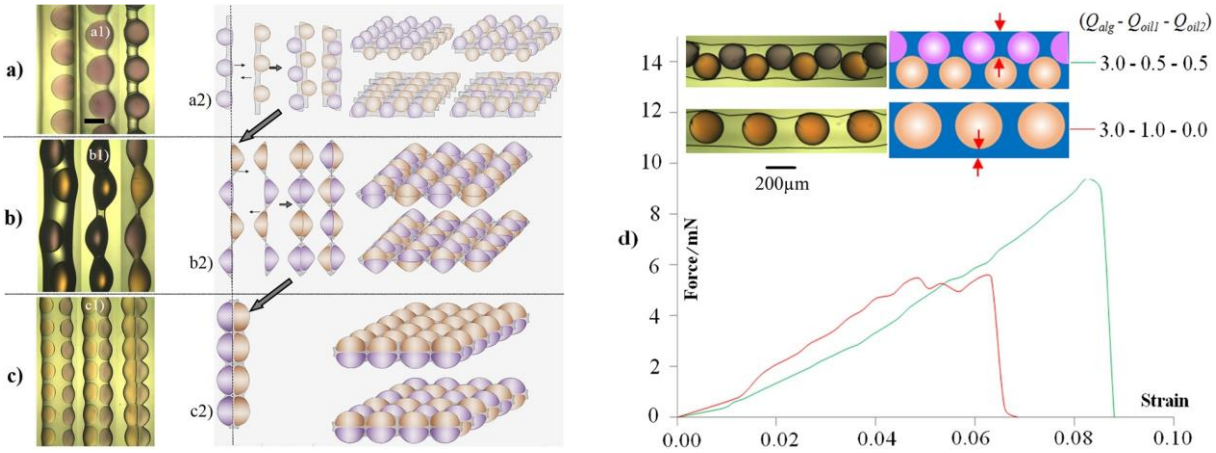

Figure 5 Micrographs of three different asymmetric oil-loaded alginate fibers **a)** simple asymmetric, **b)** alternating asymmetric, and **c)** Yanus-like, along with schematics of their arrangements into various fiber pads. The common scale bar shown in (a) is 200µm. **d)** Comparison between asymmetric fibers with single and double oil sequences, respectively, at a fixed ϕ oil (25%).

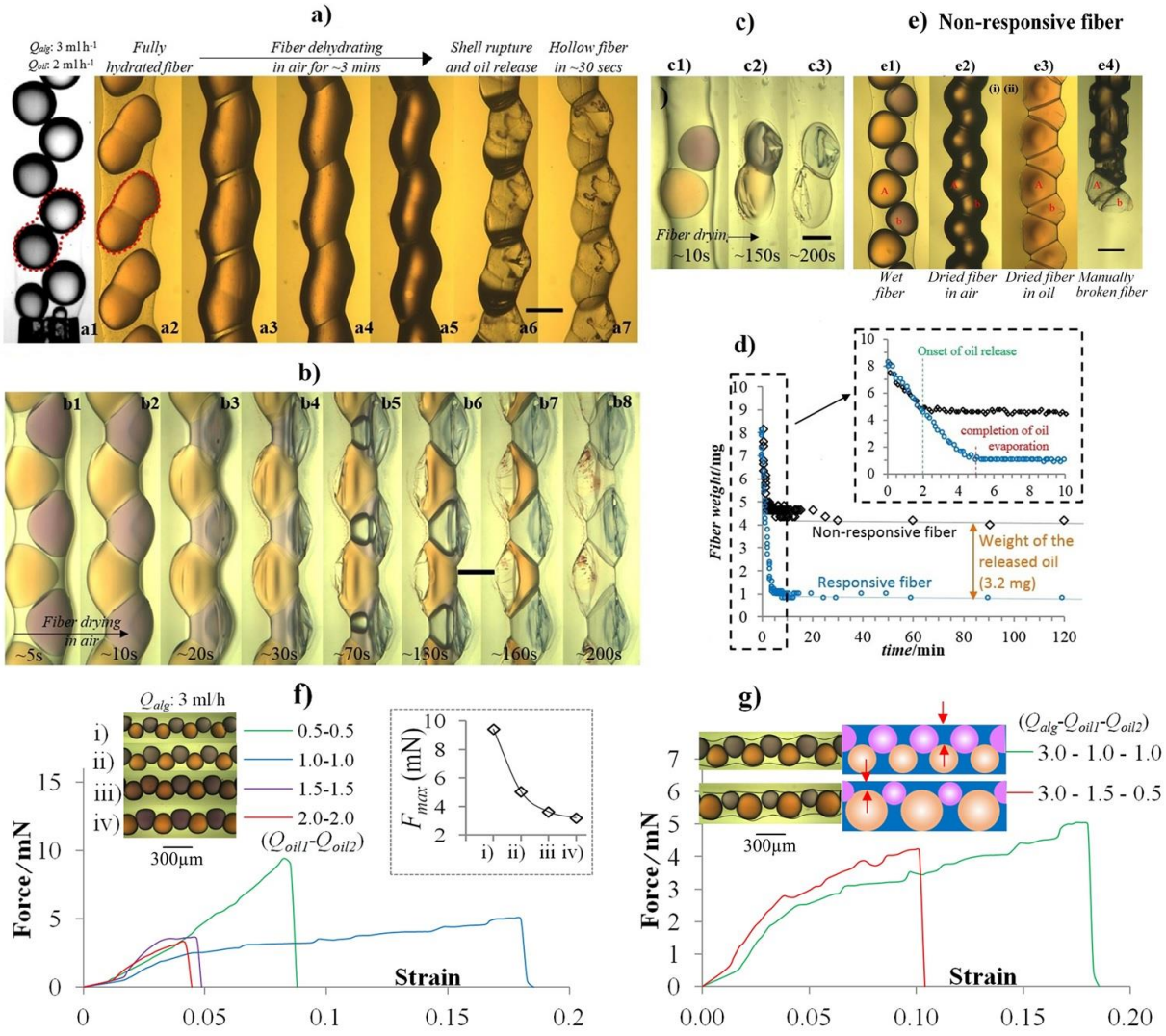

Figure 6 a) Fiber containing two asymmetric oil droplet sequences in the absence of surfactant, and their eventual paired arrested coalescence (a2) are shown. The release of oil from this dumbbell-shaped one-component oil segment is triggered by drying this microfiber (a3-a6), which eventually leaves behind a hollow microfiber, as shown in a7. **b)** The optical micrographs show the time evolution of a dehydrating microfiber containing two sequences of oil droplets added non-axisymmetrically, which are eventually released. The alginate phase contained an extremely small amount of surfactant (0.01 wt% Tween 20). **c)** The time evolution of the core-release from a sparsely loaded fiber with adjacent alternating droplets is shown. **d)** Time variation in the fiber weight for the fiber hydration-responsive fiber shown in (a). The inset graph shows a zoomed-in view of the dynamics of the dehydration (drying) at room temperature in the initial ten minutes. **e)** The micrographs show a non-responsive fiber made with 1.0 wt%

Tween 20. The alginate shell remains intact after dehydration, as visible in (e3), where the dehydrated fiber is immersed in oil. The image in (e2) is dark due to high refractive index mismatch (air outside, oil inside). A dried fiber broken by a rapid manual axial pull, showing empty adjacent segments in (e4). All scale bars are 200µm. **f)** Force-strain curves obtained via uniaxial tensile testing of four asymmetric fibers with equal adjacent spheres at different oil volume fractions, ϕ_{oil} (i-25%, ii-40%, iii-50%, iv-57%). The inset graph shows a reduction in the maximum tensile force (F_{max}) withstood by the fibers with increasing oil volume fraction. **g)** Comparison between asymmetric fibers with equal and unequal spheres, respectively, at a fixed ϕ_{oil} (40%).

Responsive alginate microfibers with asymmetric oil encapsulates, which exhibit dehydration-triggered core-release, are fabricated via a novel asymmetric encapsulation method. The fibers could also be tuned to carry and release multiple oil cargos.

Keyword: alginate microfibers, oil encapsulation, dehydration, core-release

A. S. Chaurasia, S. Sajjadi*

Flexible Asymmetric Encapsulation for Dehydration-Responsive Hybrid Microfibers

ToC figure